

Spin-orbit coupling and operation of multi-valley spin qubits

M. Veldhorst,^{1,*} R. Ruskov,² C.H. Yang,¹ J.C.C. Hwang,¹ F.E. Hudson,¹
M.E. Flatté,³ C. Tahan,² K.M. Itoh,⁴ A. Morello,¹ and A.S. Dzurak^{1,†}

¹Centre for Quantum Computation and Communication Technology,
School of Electrical Engineering and Telecommunications,
The University of New South Wales, Sydney, NSW 2052, Australia

²Laboratory for Physical Sciences, 8050 Greenmead Dr., College Park, MD 20740, USA.

³Department of Physics and Astronomy, University of Iowa, Iowa City, Iowa 52242.

⁴School of Fundamental Science and Technology, Keio University,
3-14-1 Hiyoshi, Kohoku-ku, Yokohama 223-8522, Japan.

(Dated: November 13, 2018)

Spin qubits composed of either one or three electrons are realized in a quantum dot formed at a Si/SiO₂ interface in isotopically enriched silicon. Using pulsed electron spin resonance, we perform coherent control of both types of qubits, addressing them via an electric field dependent g -factor. We perform randomized benchmarking and find that both qubits can be operated with high fidelity. Surprisingly, we find that the g -factors of the one-electron and three-electron qubits have an approximately linear but opposite dependence as a function of the applied dc electric field. We develop a theory to explain this g -factor behavior based on the spin-valley coupling that results from the sharp interface. The outer “shell” electron in the three-electron qubit exists in the higher of the two available conduction-band valley states, in contrast with the one-electron case, where the electron is in the lower valley. We formulate a modified effective mass theory and propose that inter-valley spin-flip tunneling dominates over intra-valley spin-flips in this system, leading to a direct correlation between the spin-orbit coupling parameters and the g -factors in the two valleys. In addition to offering all-electrical tuning for single-qubit gates, the g -factor physics revealed here for one-electron and three-electron qubits offers potential opportunities for new qubit control approaches.

Silicon is known among the semiconductors to have small spin-orbit coupling (SOC), a beneficial fact for silicon quantum computing, since charge noise is largely decoupled from information stored in the spin [1]. Furthermore, silicon can be isotopically enriched and chemically purified to ²⁸Si, thereby removing nuclear spin background fluctuations and so silicon is often referred to as a semiconductor vacuum [2]. These two facts have motivated intense research on silicon qubits, leading to recent realizations of single-qubit [3–7] and two-qubit [8] logic gates. Despite the small SOC in isotopically purified silicon quantum dots, the small tunability of the g -factor via gate-controlled electric fields allows one to electrostatically turn on and off the spin rotations that constitute single-qubit gates [7–9], thereby providing an important tool for quantum computation.

The low-energy subspace in silicon quantum dot (QD) systems is governed by two spin-degenerate valley states. When these valley states are quasi-degenerate, qubit operation becomes complex [6], and the coupling of qubits is even more challenging [10]. However, the valley states can be separated using a vertical electric field and the sharp potential of an interface [7, 11], and their energy separation can be electrically controlled over several hundreds of μeV . While one-electron spin qubits are naturally operated in the lowest valley state [6, 7], it is intriguing to consider the potential performance of qubits operated in the higher valley state, which is also known to have a long spin lifetime if orbital relaxation can be suppressed [11]. When spatial confinement in the QD is strong, the orbital excited states are lifted high in energy and qubit operation in the upper valley state is possible by populating three electrons in the quantum dot. In this mode two electrons

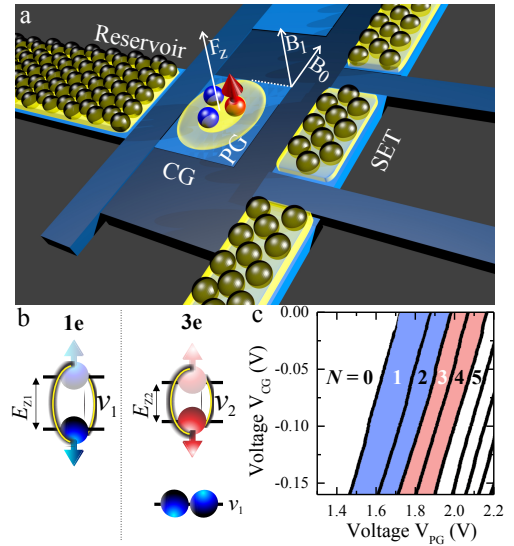


FIG. 1: (a) Schematic representation of the quantum dot system. The quantum dot is defined using the confinement gate CG and plunger gate PG and the yellow shading represents the regions where electrons are accumulated, with F_z the perpendicular electric field direction. ESR control is via a dc magnetic field $B_0 = 1.4\text{ T}$ (in the Si [110] in-plane direction) and an ac magnetic field B_1 . (b) The quantum dot qubit can be operated using the spin states of one electron, or using three electrons, where two electrons (blue) occupy the lowest energy valley state and the third electron (red) is in the higher energy valley state. (c) Charge stability diagram showing the electron occupancy N in the quantum dot, measured with a nearby SET.

form a singlet in the lower valley state and the third electron

is operated in the upper valley (see Fig. 1a and 1b). It has been suggested that such multi-electron qubits could enhance the gate fidelity, due to partial screening of electrical noise [12].

In this letter, we demonstrate high-fidelity operation of one- and three-electron spin qubits, operated in the lower and upper valley, respectively. Using pulsed electron-spin-resonance (ESR) we map out with high precision the qubit frequency as a function of the applied perpendicular electric field, controlled with electrostatic gates. We experimentally demonstrate and theoretically explain how inter-valley spin-orbit coupling at the Si/SiO₂ interface results in an opposite dependence of the g -factor for the two valleys, that is correlated with the corresponding dependence of the 2D Rashba and Dresselhaus spin-orbit coupling in each valley. We also present randomized benchmarking on both qubit systems, showing they are capable of fidelities above 99%, approaching the surface code thresholds for fault-tolerant quantum computing [13].

The QD structure is fabricated on an epitaxially grown, isotopically purified ²⁸Si epilayer with a residual concentration of ²⁹Si at 800 ppm [2]. The aluminum gates are fabricated with electron-beam lithography using a multi-level gate stack silicon metal-oxide-semiconductor (SiMOS) technology [14], see Fig. 1. The charge stability diagram of the quantum dot is shown in Fig. 1c. We use ESR to control the one-electron qubit [7] and the three-electron qubit, see Fig. 2. From a Ramsey sequence we find a long dephasing time $T_2^* = 70 \mu\text{s}$, which is slightly less than we have previously measured for the one-electron qubit, which had $T_2^* = 120 \mu\text{s}$ [7].

We have demonstrated electric field control over the resonance frequency ν_{ESR} of the one-electron qubit [7], showing tunability over several MHz that appears linear in electric field, corresponding to more than 3000 times the 2.4 kHz ESR line-width. We find that spin-valley mixing of the QD eigenstates due to interface roughness [11] would predict a modification of the electron g -factor that is two orders of magnitude smaller than is found experimentally, together with a non-linear dependence close to the anticrossing point of the spin-valley states that we do not observe. Here we propose and analyze a model where the g -factor modification proceeds via inter-valley spin-flip tunneling, mediated by the strong z -confinement at the interface. The Si/SiO₂ (001) interface of silicon MOS quantum dots can be described with a Hamiltonian that consists of a bulk term \mathcal{H}_0 and an interface term \mathcal{H}_{if} . The reduction of the bulk Si crystal symmetry at the interface, in the presence of strong perpendicular electron confinement induced by an applied electric field F_z , lifts the six-fold valley degeneracy, leaving two low-lying Δ -valleys at $\pm k_{0z}$. These are then mixed via enhanced inter-valley tunneling due to the strong z -confinement at the interface [15, 16]. The consequent effective two-valley Hamiltonian acts on the four-component vector $(\Phi_{z,\uparrow}(r), \Phi_{z,\downarrow}(r), \Phi_{-\hat{z},\uparrow}(r), \Phi_{-\hat{z},\downarrow}(r))^T \equiv \Phi(r)$, where

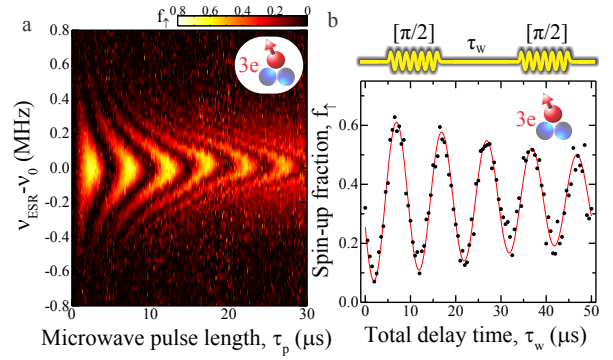


FIG. 2: Demonstration of qubit control of the three-electron qubit. (a) 2D colour map showing Rabi control of the spin-up fraction f_{\uparrow} , by varying the microwave pulse length and the microwave driving frequency ν_{ESR} . We have subtracted a reference frequency $\nu_0 = 39.045$ GHz (corresponding to $g = 1.9908$) for clarity. (b) Ramsey fringes, obtained by varying the waiting time in between two ESR $\pi/2$ pulses. The decay in the spin-up fraction f_{\uparrow} corresponds to $T_2^* = 70 \mu\text{s}$. The confinement gate voltage is $V_C = -0.2$ V.

the bulk part (spin and valley degenerate) is given by

$$\mathcal{H}_0 = \left[\sum_{j=x,y,z} \frac{\hbar^2 \hat{k}_j^2}{2m_j} + U_{x,y} + U_z \right] \times \hat{I}_4 \quad (1)$$

with the quasi-momentum operators $\hat{k}_j \equiv -i\partial_j$; and $U_{x,y} = \frac{m_t}{2} \omega_0^2 (x^2 + y^2)$ and $U_z = |e|F_z z$ are the in-plane and perpendicular confinement electron potentials, respectively. Here m_l, m_t are the Si effective Δ -valley electron masses, $|e|$ is the electron charge, and \hbar is the reduced Planck constant. Taking into account the large band offset of Si/SiO₂, the interface term is

$$\mathcal{H}_{if} = -\frac{\hbar^2}{2Rm_l} \delta(z - z_0) - i \frac{\hbar^2}{2m_l} \delta(z - z_0) \hat{k}_z + \delta(z - z_0) \hat{V}_{if}(k), \quad (2)$$

where R is a parameter with dimension of length, characterizing an abrupt interface [17, 18], and $|R| \ll l_z \ll l_D$; here $l_z = (\hbar^2/2m_l|e|F_z)^{1/3}$ and $l_D = (\hbar/m_t\omega_0)^{1/2}$ are the perpendicular and in-plane confinement lengths (assuming much stronger \hat{z} -confinement). For $R \approx 0$ the interface Hamiltonian (Eq. 2) corresponds to the standard infinite boundary condition (BC) $\Phi(z)|_{z=z_0} = 0$, while for finite R it generates spin and valley mixing at the interface, $z \gtrsim z_0$. Following the symmetry reasoning of Refs. [19–21] the spin-valley mixing interface matrix $\hat{V}_{if}(k)$ can be expressed via the C_{2v} invariants $H_R(k) = \sigma_x k_y - \sigma_y k_x$, $H_D(k) = \sigma_x k_x - \sigma_y k_y$, resulting in

$$\hat{V}_{if}(k) = \begin{bmatrix} A(k) & V\hat{I}_2 + B(k) \\ V^* \hat{I}_2 + B^\dagger(k) & A(k) \end{bmatrix}. \quad (3)$$

In Eq. (3) the 2×2 block-diagonal element $A(k) \equiv s_D H_D(k) + s_R H_R(k)$ corresponds to *intra-valley* spin-flipping transitions, while the off-diagonal elements $V\hat{I}_2$,

$B(k) \equiv \chi_D H_D(k) + \chi_R H_R(k)$ are related to *inter-valley* tunneling (in momentum space) with no spin-flipping or with a spin-flipping process. Since experimentally the valley splitting ($\sim |V|$) is generally large with respect to the spin-flipping terms, it makes sense to diagonalize with respect to the leading V -matrix element and via a unitary transformation we find

$$\hat{V}_{\text{if}}^{\text{U}}(k) = \begin{bmatrix} |V| + A + \frac{1}{2}B_d & \frac{1}{2}B_{\text{off}} \\ \text{h.c.} & -|V| + A - \frac{1}{2}B_d \end{bmatrix}. \quad (4)$$

This matrix is approximately diagonal in the valley basis $|v_1\rangle, |v_2\rangle$, with a calculated valley splitting energy $E_{\text{VS}} = 2|V|R^2|\varphi'(0)|^2 = 2|V|R^2l_z^{-3} \propto F_z$. We neglect the off-diagonal contribution $B_{\text{off}} \equiv B - B^\dagger e^{2i\phi_V}$ in Eq.(4), since it is suppressed as $\sim 1/E_{\text{VS}}$ and E_{VS} is typically several hundreds of μeV in MOS quantum dots [7, 11]. Thus, in the valley subspaces $|v_1\rangle, |v_2\rangle$, one can consider two independent boundary conditions as in Eq.(2), with spin-flipping interface matrices $\hat{V}_{v1,v2} = A \mp \frac{1}{2}B_d \equiv A \mp \frac{1}{2}(Be^{-i\phi_V} + B^\dagger e^{i\phi_V})$, in which the inter-valley spin-flip tunneling element changes sign between $v1$ and $v2$.

The effective 2D spin-orbit Hamiltonians (proportional to the Rashba and Dresselhaus forms, $H_R(k), H_D(k)$) are straightforwardly calculated from Eq.(2), with the corresponding 2D SOC parameters changing sign as well:

$$\begin{aligned} \alpha_{R;v1,v2} &= 2[s_R \mp |\chi_R| \cos(\phi_R - \phi_V)] R^2 |\varphi'(0)|^2 \\ \beta_{D;v1,v2} &= 2[s_D \mp |\chi_D| \cos(\phi_D - \phi_V)] R^2 |\varphi'(0)|^2. \end{aligned} \quad (5)$$

The scaling of the spin-orbit terms with the electric field F_z is linear, as is the valley splitting, E_{VS} . Here, we have introduced the phases ϕ_R and ϕ_D for the Rashba and Dresselhaus terms and $\varphi'(0)$ is the derivative of the z -component of an eigenstate of the bulk Hamiltonian \mathcal{H}_0 . These results are similar to the strong field limit results of Ref. [21].

Explicit calculation of the g -factor change, based on the interface Hamiltonian Eq.(2) and the fact that an in-plane magnetic field mixes the perpendicular and in-plane motion, shows that the in-plane g -factor renormalization δg is proportional to α_R, β_D . For the magnetic field parallel to the [110] direction (as in the experiment) one obtains the expression:

$$\delta g_{v1,v2} = -\frac{(\alpha_{R;v1,v2} - \beta_{D;v1,v2})|e|}{\hbar\mu_B} \langle z \rangle \quad (6)$$

where μ_B is the Bohr magneton and $\langle z \rangle \simeq 1.5587 l_z$ is an average of the z -motion in the lowest subband, see Eq.(1). The g -factor scales as $F_z^{2/3}$, which is close to a linear scaling over the range ($\sim 10\%$) of the experimentally applied electric fields, see Fig. 3b.

We therefore expect from Eq.(6) that the renormalization δg will be of opposing sign for the two valleys, following the sign change of the SOC parameters in Eq.(5). In particular, the change will be exactly opposite for zero intra-valley spin-flip coupling, $s_R, s_D = 0$:

$$\delta g_{v1} = -\delta g_{v2}. \quad (7)$$

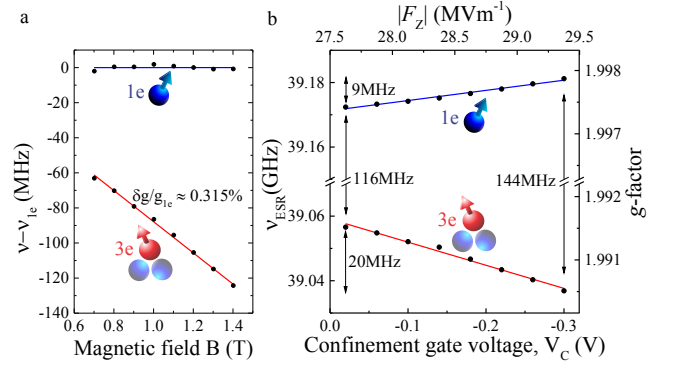


FIG. 3: (a) Magnetic field dependence of the resonance frequency of the one- and three-electron qubit, with $F_z = 28.25 \text{ MV/m}$. The experimental data of both qubit systems has been subtracted by the g_{1e} -factor for comparison and we have calibrated the dc magnetic field using the crossing point of the one- and three-electron qubit resonance frequencies. We find $g_{1e} = 1.9975$ and $g_{3e} = 1.9912$. (b) Gate tuned electric field control over the valley g -factor at $B_0 = 1.4015 \text{ T}$.

Relatively smaller corrections due to non-zero intra-valley spin flipping, $s_R, s_D \neq 0$ will generally violate Eq. (7), leaving the g -factor changes opposite in sign, but with different absolute value, $|\delta g_{v1}| \neq |\delta g_{v2}|$.

To observe this experimentally, we control the quantum dot electric field via the plunger gate PG and the confinement gate CG , see Fig. 1. In Fig. 3a we show the magnetic field dependence and in Fig. 3b we show electrical control over the qubit resonance frequency ν_{ESR} . The opposite electric field dependence of the g -factor for the two valleys is in qualitative agreement with the prediction of Eq.(7). Since the resonance frequency of the one-electron qubit increases with the electric field, while the resonance frequency of the three-electron qubit decreases (see Fig. 3b), we infer from Eq.(6) that the Rashba and Dresselhaus contributions are in this experiment subject to the constraints: $\delta\chi_{\text{inter-val}} \equiv |\chi_R| \cos(\phi_R - \phi_V) - |\chi_D| \cos(\phi_D - \phi_V) > 0$, $\delta s_{\text{intra-val}} \equiv s_R - s_D < 0$. The change in sign of δg is evidence that the inter-valley spin-flip contributions dominate the intra-valley spin-flip processes and from the δg -dependence we estimate the ratio $\delta\chi_{\text{inter-val}}/|\delta s_{\text{intra-val}}| \approx 2.6$. This observation is consistent with tight-binding calculations on SiGe quantum wells [21], which predict that the inter-valley transitions can be about an order of magnitude larger than the intra-valley transitions. Interestingly, the values and signs of the SiGe parameters, as substituted in Eqs.(5) and (6), reproduce also the correct qualitative behavior of δg_{v1} (δg_{v2}) that increases (decreases) with the applied electric field F_z , as is observed experimentally in Fig. 3b. However, the experimental ratio of the g -factor changes is $|\delta g_{v2}|/|\delta g_{v1}| \simeq 2.2$, while that calculated with the Si/SiGe parameters is ~ 1 . Such differences can be expected due to the much greater band-edge offset in Si/SiO₂, disorder [22], and built-in electric fields which may also influence the theoretical results.

In order to explore the qubit performance for quantum com-

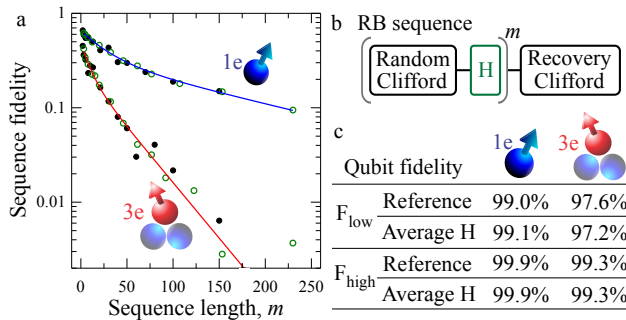


FIG. 4: Clifford based randomized benchmarking (a) Sequence fidelity as a function of the sequence length and (b) schematic representation of randomized benchmarking, where H is an interleaved test gate. In (a), the black filled circles correspond to standard randomized benchmarking and the green open circles to the average of the single qubit gates $[I, \pm X, \pm \frac{1}{2}X, \pm Y, \pm \frac{1}{2}Y]$, obtained by interleaved randomized benchmarking and normalizing the sequence length with $2.875/1.875$, such that it matches the average Clifford gate length. Both data sets are fitted with a two-fidelity model (see text) and the results are shown in (c), where the standard error is smaller than the corresponding gate error.

putation, we have performed (interleaved) randomized benchmarking (RB) [23, 24] on the one-electron qubit [7] and three-electron qubit, and all results are shown in Fig. 4. In order to eliminate the free fitting parameter B , which is a constant offset parameter present in standard RB fits, we plot the sequence fidelity combination $F = F_{\uparrow} + F_{\downarrow} - 1$, which approaches zero for infinite sequence length when the assumptions of RB hold [25]. When the noise is gate independent, an exponential decay is expected for both standard and interleaved randomized benchmarking. However, when low-frequency noise is present, non-exponential decays arise [25]. This non-exponential decay is due to slow drifts in the resonance frequency, such that the time ensemble is averaged over sequences with small detuning (resulting in a high fidelity, F_{high} , and a slow exponential decay) and large detuning (resulting in a low fidelity, F_{low} , and a fast exponential decay).

When such low-frequency noise is present, the fidelity varies over time and we use a two-fidelity model to analyse the data [25]. We have fitted the data using $F = A(p^m + q^m)$, where A quantifies the SPAM error and p and q are two polarization parameters, and in Fig. 4c we show the corresponding fidelities. The three-electron qubit has a relatively low fidelity when the noise causes a large detuning ($F_{low} \approx 97\%$). However, when the microwave driving frequency is on resonance, both qubits have a fidelity above certain thresholds for fault tolerant quantum computing [13]; the average single-gate fidelity being $F_{high} = 99.9\%$ for the one-electron qubit system and $F_{high} = 99.3\%$ for the three-electron qubit system. While the three-electron qubit initially shows a non-exponential decay, for higher m the decay approaches a pure exponential, indicating that low frequency noise has little impact in this range. Since both qubit systems are operated with the same setup, we expect similar calibration errors. This exponential

decay is therefore likely due to high-frequency noise.

The faster decay of the sequence fidelity of the three-electron vs. one-electron qubit is consistent with a larger sensitivity to electrical noise, as revealed by the larger frequency shift with gate voltage, $|\delta\nu_{3e}/\delta V| \approx 2.2|\delta\nu_{1e}/\delta V|$, shown in Fig. 3b. The frequency detuning caused by electrical noise results in rotations around the z -axis of the qubit Bloch sphere and opposite to the Rabi driving axis. By taking the small-angle approximation, we find that the gate error increases with the square of the noise term. This results in an error rate that is around 5 times larger for the three-electron qubit, comparable with the difference in fidelities between the one-electron and three-electron qubits. It is therefore likely that both qubits are ultimately limited by high-frequency electrical noise.

The recent realizations of single- and two-qubit gates using isotopically purified silicon quantum dots [7, 8] are now revealing the early promises of silicon as a platform for quantum computation and the possibility of qubit operation with either one-electron or three-electrons allows more flexibility in scaling these systems. The ultra-narrow spin-resonance linewidth associated with the long coherence times of these qubits has pushed silicon into a new regime, where the weak spin-orbit coupling in silicon becomes not only visible, but also forms a new tool to control the spin states, as shown here. The remarkably large electric field control in SiMOS quantum dots provides further motivation to explore spin-orbit coupling in silicon for qubit control and spin manipulation.

Acknowledgments: The authors thank L.M.K. Vandersypen for insightful discussions. The authors acknowledge support from the Australian Research Council (CE110001027), the US Army Research Office (W911NF-13-1-0024) and the NSW Node of the Australian National Fabrication Facility. M.V. acknowledges support from the Netherlands Organization for Scientific Research (NWO) through a Rubicon Grant. The work at Keio has been supported in part by the Grant-in-Aid for Scientific Research by MEXT, in part by NanoQuine, in part by FIRST, and in part by JSPS Core-to-Core Program.

* Electronic address: M.Veldhorst@unsw.edu.au

† Electronic address: A.Dzurak@unsw.edu.au

- [1] F. Zwanenburg *et al.*, Rev. Mod. Phys. **85**, 961-1019 (2014).
- [2] K.M. Itoh and H. Watanabe, MRS Communications **4**, 143-157 (2014).
- [3] B.M. Maune *et al.*, Nature **481**, 344 (2012).
- [4] J.J. Pla *et al.*, Nature **489**, 541-545 (2012).
- [5] D. Kim *et al.*, Nature **511**, 70-74 (2014).
- [6] E. Kawakami *et al.*, Nature Nanotechnology **9**, 666-670 (2014).
- [7] M. Veldhorst *et al.*, Nature Nanotechnology **9**, 981 (2014).
- [8] M. Veldhorst *et al.* arXiv:1411.5760.
- [9] A. Laucht *et al.*, Science Advances **1**, e1500022 (2015).
- [10] D. Culcer, L. Cywinski, Q. Li, X. Hu, and S. Das Sarma, Phys. Rev. B **82**, 155312 (2010).
- [11] C.H. Yang *et al.*, Nature Comm. **4**, 2069 (2013).
- [12] E. Barnes, J.P. Kestner, N.T.T. Nguyen, and S. Das Sarma, Phys

- Rev. B **84**, 235309 (2011).
- [13] A.G. Fowler, M. Mariani, J.M. Martinis, and A.N. Cleland, Phys. Rev. A **86**, 032324 (2012).
- [14] S.J. Angus, A.J. Ferguson, A.S. Dzurak, and R.G. Clark, Nano Lett. **7**, 2051 (2007).
- [15] F.J. Ohkawa, Sol. Stat. Commun. **26**, 69 (1978).
- [16] T. Ando, A.B. Fowler, and F. Stern, Rev. Mod. Phys. **54**, 2 (1982).
- [17] V.A. Volkov and T.N. Pinsker, Surface Science **81**, 181 (1979).
- [18] F.T. Vasko, JETP Letters **30**, 541 (1979).
- [19] M.O. Nestoklon, L.E. Golub, and E. L. Ivchenko, Phys. Rev. B **73**, 235334 (2006).
- [20] L.E. Golub and E.L. Ivchenko, Phys. Rev. B **69**, 115333 (2004).
- [21] M.O. Nestoklon, E.L. Ivchenko, J.M. Jancu, and P. Voisin, Phys. Rev. B **77**, 155328 (2008).
- [22] M. Friesen and S.N. Coppersmith, Phys. Rev. B **81**, 115324 (2010).
- [23] E. Knill *et al.*, Phys. Rev. A **77**, 012307 (2008).
- [24] E. Magesan *et al.*, Phys. Rev. Lett. **109**, 080505 (2012).
- [25] M. Fogarty *et al.*, ArXiv:150205119.